*Omega-P, Inc.*
291 Whitney Avenue, Suite 401
New Haven, CT 06511

**FINAL REPORT TO DEPARTMENT OF ENERGY**
**FOR PHASE I GRANT DE-SC0009607**

# ELECTRON-BEAM SWITCHES FOR A HIGH PEAK POWER SLED-II PULSE COMPRESSOR

J. L. Hirshfield, Principal Investigator
tel: (203) 432-5428, e-mail: jay.hirshfield@yale.edu

## TABLE OF CONTENTS



November 18, 2015

## I. INTRODUCTION

The DoE 2012 SBIR/STTR Phase I Program Solicitation requested grant applications under Topic 34c RADIO FREQUENCY ACCELERATOR TECHNOLOGY FOR HIGH ENERGY ACCELERATORS, *Radio Frequency Power Sources and Components.* Therein, grant applications were sought to develop active RF pulse compression systems capable of handling high peak powers (for example, > 300 MW) with pulse widths of about 300 nanoseconds at X-band. Omega-P, Inc. submitted a proposal in response, and was awarded Phase I grant DE-SC0009607. This document reports on the Phase I project.

A means to provide extra-high peak power rf pulses is through use of a pulse compressor to multiply the peak output power from a high-power klystron. The SLED-II compression system allows an increase in peak rf power by several times by shortening the pulse from the klystron [1]. This system is fully passive. Microwave energy is stored in two low-loss resonant delay lines. The system is shifted from the regime of energy storage to the regime of energy discharge by reversing the phase of the klystron output during the pulse. Such a system at 2.856 GHz has been used successfully at the SLC, with parameters as follows: compression ratio $C$ = 6, power gain $M$ = 4.1 and efficiency $\eta$ = 68%. But a passive SLED-II system may not be attractive for high gradient X-band linacs that require $M$ > 4, since the efficiency of compression decreases as the compression ratio is increased.

A remedy to this problem was proposed in1996 by Tantawi, Ruth and Vlieks, namely the active SLED-II system [2]. Their concept is to shift from energy storage to energy discharge by changing both the phase of the rf input and the coupling coefficient to the delay line. In the existing SLED-II, the delay line coupling iris has a constant reflection coefficient $R$. Replacing the iris with an active element makes it possible to create an active SLED-II. If, for example, rapid electrical control shifted $R$ from $R_o$ = 0.8-0.96 to $R_d$ = 0.2-0.4, it would—in principle—allow pulse compression with $C$ = 8-16, $M$ = 7-12, and $\eta$ = 84-82%, depending on losses in the resonant delay lines.

Parameters of an active SLED II operating with simultaneous reversal the phase of the input signal and changing the coupling coefficient from $R_0$ = 0.85 to $R_d$ = 0.11 is shown in Fig.1. The figure shows the calculated dependencies of power gain $M$ and compression efficiency $\eta$ on compression ratio $C$, for various round trip power losses. The maximum efficiency predicted for $C$ = 12-16; where $M$ = 10-12. Hence to obtain maximum efficiency, the klystron pulse duration for the SLED-II delay line length $L$ = 35 m would need to be about 2.5 μs. To obtain the highest power gain using an existing X-band SLAC klystron with 1.6 μs pulses, the delay line would need to be shortened to $L$ = 16-18 m, and the output pulse duration would be about 90 ns, with $C$ = 16.

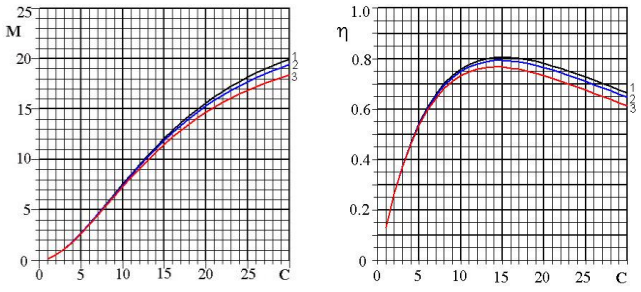


(*a*) (*b*)

Fig. 1. Calculated dependencies of the power gain (*a*) and efficiency (*b*) on the compression ratio $C$, for different values of round trip power loss: *1* - α = 0.3%, *2* – α = 0.6%, *3* – α = 1.2%.

During and preceding Phase I, Omega-P demonstrated triggered electron-beam switches on the $L$ =2 m dual-delay-line X-band pulse compressor at Naval Research Laboratory (NRL); results of that experiment were reported in 2013 in *Physical Review Letters* [3]. In those experiments, with input pulses of up to 9 MW from the Omega-P/NRL X-band magnicon, output pulses having peak powers of 140-165 MW and durations of 16-20 ns were produced, with record peak power gains $M$ of 18-20. Below, switch designs are described based on the successful results from those experiments that

should be suitable for use with the existing SLAC SLED-II delay line system, to demonstrate $C = 9$, $M = 7$, and $\eta \approx 78\%$, yielding 173 ns compressed pulses with peak powers up to 350 MW, with input from a single 50-MW klystron. Shortening the delay lines by half to 17 m could allow operation with $M = 12.5$ and peak powers up to 600 MW in 86 ns pulses; but we are at present not counting on SLAC being ready to reconfigure SLED-II.

Successful future demonstration of an active SLED-II with generation of 173 ns wide, 175-350 MW X-band pulses requiring input from only a single 50-MW klystron could lead to establishment of a unique-in-the-world high-power test facility at SLAC for future high-power X-band R&D. Other uses for active X-band pulse compression include one prominent example: namely, a 100-MeV accelerator proposed for e-beam cancer therapy [4], as a more rapid and cost-effective alternative to proton therapy.

Advancements in nuclear and high-energy physics have, in the years since WWII, brought enormous practical benefit to the US public in general, and to the US scientific community in particular. Widely-dispersed pay-offs include fast integrated-circuit electronics, accelerators for radiotherapy and industrial processing, nuclear power, and the internet. Successful completion of the project proposed here will allow generation very high power microwave pulses (several hundred megawatts at X-band) in a system powered by a single well-established SLAC klystron. Use of such high-power pulses can range from basic scientific studies that are relevant to developing the next high-energy electron-positron collider for discoveries in high-energy physics, to advanced radars including versions for underground exploration, for Homeland Security applications, and for industrial processes. Another exciting prospect for an actively-compressed X-band pulse—as stated above—is in radiation therapy, where a 100 MeV e-beam could be rapidly scanned across a tumor in a much shorter time than is currently required for proton therapy [4]. This would subject patients to much shorter exposure time with reduced collateral damage than with proton therapy, from an accelerator system requiring only a single moderate-power klystron with a much smaller footprint and lower cost than existing proton accelerators. In the near-term, a permanent installation at SLAC could evolve that, at little additional public cost, provide a stand-along test stand to enable development of the range of applications mentioned. It is not inconceivable that complete turn-key systems could be manufactured and delivered to customers who wished to operate the system independent of National Laboratory priorities, including use on future developments of proprietary technologies with the potential for realization of profitable revenues and associated job creation.

## II. TECHNICAL APPROACH

Full background material on active RF pulse compression is given in our Phase I proposal and our recent publications [5-8]. New results are presented here.

### IIa. Experiment with active microwave pulse compressor using an electron-beam triggered switch

Several active rf pulse compression systems have been developed and tested at high-power levels by us using the 11.4 GHz Omega-P/NRL magnicon [3,6,7]. In these experiments, plasma [6,7] and electron beam (e-beam) [3] switches were used as the active elements. Best results were found with a two-channel compressor using e-beam switches [3]. A diagram of the set-up at NRL is in Fig. 2. Each storage cavity comprised an input horn, a cylindrical waveguide 210 cm long and 80 mm in diameter, and the switch, sketched in Fig. 3. In this configuration, rf energy is stored in the high-$Q$ $TE_{02}$ mode of two parallel-fed cavities, and switched out in the $TE_{01}$ mode. Switching is based on a sharp increase in $TE_{02} \rightarrow TE_{01}$ mode conversion coefficient, when an e-beam is injected into the switch resonator. Two channels allow isolation of the rf source from power reflected during energy storage, avoiding a high power, evacuated circulator. The compressor comprises two identical channels; the principle of operation is shown in Fig. 3a.

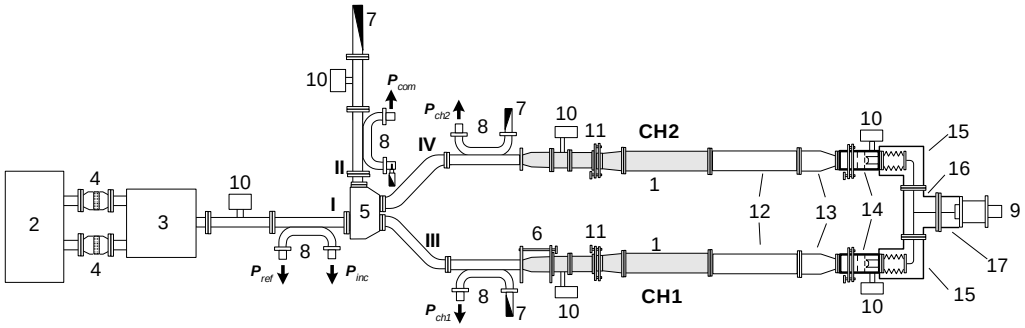


Fig. 2. Schematic diagram of the set-up used at NRL for tests of two-channel pulse compressor with Omega-P switches using e-beam triggering: (1) single-channel; (2) magnicon; (3) combiner; (4) output window; (5) 3-dB hybrid coupler; (6) phase shifter; (7) matched load; (8) 55.5-dB directional coupler; (9) high voltage generator; (10) ion pump; (11) mode converter, (12) cylindrical waveguide, (13) taper, (14) switch, (15), (16), (17) screen.

Microwave energy is fed to the input in the $TE_{01}$ mode of circular waveguide. The compressor consists of coupling device (1) (input and output waveguides in which the $TE_{02}$ mode is cut off), input horn (2), a section of cylindrical waveguide (3), and switch (4-9). Input horn, cylindrical waveguide, and switch form a storage cavity for the $TE_{02}$ mode. The cylindrical waveguide (3) includes a section of variable length which can be mechanically adjusted to tune the cavity to the working frequency. In the regime of energy storage, a small fraction (~1–3%) of the $TE_{01}$ mode power is converted with the aid of the conical taper (4) into the $TE_{02}$ mode. This mode is completely reflected from input horn (2). As a result, the microwave energy is stored in the cavity in the $TE_{02}$ mode.

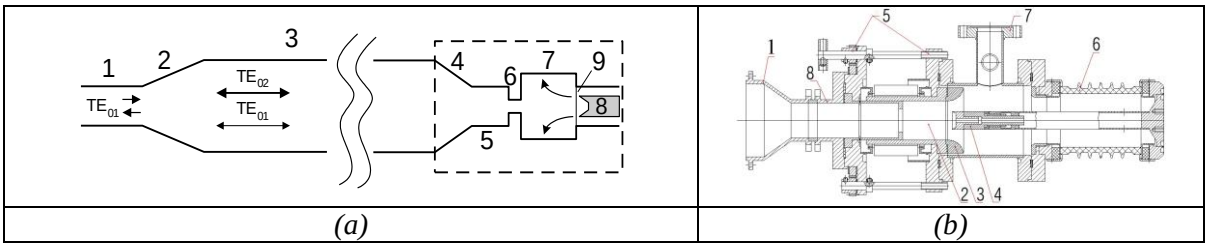


*(a)* *(b)*

Fig. 3. (a) Schematic diagram of the single-channel compressor: 1 – input $TE_{01}$ mode waveguide, 2 – input horn, 3 – cylindrical cavity, 4 – conical taper, 5 – waveguide section, 6 – diaphragm, 7 – $TE_{012}$-mode switch resonator, 8 – cathode, 9 – anode plate; (b) Scheme of the e-beam switch: 1- conical taper, 2 – switch resonator, 3 – anode (copper disk with slits), 4 - cathode, 5 – adjustment device, 6 - isolator, 7 – pumping, 8 - waveguide section.

The switch consists of a taper (4), in which modes are converted ($TE_{02} \rightarrow TE_{01}$ and $TE_{01} \rightarrow TE_{02}$), and waveguide section (5) of variable length with its length chosen in such a way as to ensure that the $TE_{01}$ modes reflected from cone (4) and resonator (7) sum up in phase opposition. As a result, the total coefficient of the $TE_{02} \rightarrow TE_{01}$ mode conversion in the switch amounts to 2–3%. Switch resonator (7) is formed by movable diaphragm (6), a section of the cylindrical waveguide and output diaphragm (9), which acts as the anode. For the penetration the e-beam into the resonator (7) a slit was cut in the anode at some distance from its center (9), and situated directly opposite the sharp edge of the cathode (8) corresponding to the field maximum in the $TE_{01}$ mode excited in the switch resonator. The front wall of the anode acted simultaneously as a wall of the switch resonator. Calculations of the amplitude of electric field in the storage cavity and the switch in regime of energy storage calculated by FDTD method [8] showed that the storage cavity $Q$-factor $Q_L \geq 104$ can be achieved, when the $Q$-factor of the switch resonator is $Q_S \approx 200\text{-}500$. The measured loaded $Q$-factors of each storage cavity of the compressor channels were $Q_{L1} \approx Q_{L2} \approx (2\text{-}3)\times 10^4$. The phase of the signal reflected from the switch resonator is strongly dependent on whether the cavity is in or out of

resonance [9]. Therefore, if a resonator is detuned (7), after initially being tuned to resonance, the phase of the signal reflected from the cavity changes by ~180° and the $TE_{01}$ modes reflected from conical taper (4) and resonator (7) start summing up in phase. Now the $TE_{02} \rightarrow TE_{01}$ conversion coefficient increases to 100% and microwave energy stored in the compressor cavity in the $TE_{02}$ mode is emitted in the $TE_{01}$ mode.

Characteristics of the microwave pulse compressor with e-beam switch triggering were experimentally studied using the Omega-P/NRL multi-MW X-band magnicon [7]. A 100 kV, 100 ns pulse was fed simultaneously to both switch cathodes, and intense e-beams were injected into the switch resonators. As a result, microwave energy stored in the cavities in the $TE_{02}$ mode was emitted through the input horns in the $TE_{01}$ mode. Typical traces of compressed pulses are shown in Fig. 4.

In these experiments, output pulses of 140-165 MW peak power were produced with power gains of 18-20 and durations of 16-20 ns, using drive powers of up to 9 MW. [The compressed pulse width was limited by the 2-m length of the delay lines.] Efficiency of compression, defined as the ratio of the energy in the compressed pulse to the energy in the incident pulse, reached 50%. High stability and repeatability of the shape of compressed pulses was observed. Thus the experiments showed that a switch based on mode conversion and employing e-beam triggering has great potential. We have concluded that these switches are suitable to be active elements in an active SLED II system.

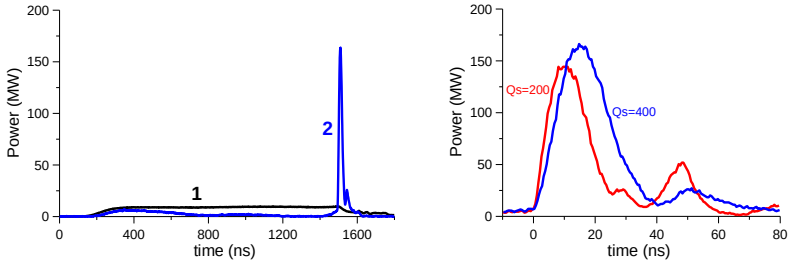


Fig. 4. Oscilloscope traces of the (1) incident and the (2) compressed pulse: (a) incident power – 9 MW, power of the compressed pulse - 165 MW, compression ratio - 18.3; (b) envelope of compressed pulses at different quality QS of switch resonator.

### IIb. Possible electron beam switch designs for an active SLED-II system

Based on our successful tests at NRL of the microwave pulse compressor with e-beam switch triggering using the 11.4 GHz Omega-P/NRL magnicon [7], we proposed for Phase I to develop and study an e-beam switch which could allow realization of an active SLED II system. During Phase I two different versions of e-beam switches based on the results described above were studied. The first version invokes changing the coupling coefficient of the delay line, as in the NRL experiment [4]. The iris of the SLED II delay line is replaced by the switch, with the rest of the arrangement as in Fig.2. The resonant delay line is tuned to $f_0$ = 11.424 GHz by moving the short circuits at the end of the delay lines, and is excited at the $TE_{01}$ mode of circular waveguide. The e-beam switch itself consists of a reflector and an iris (or diaphragm) as is shown schematically in Fig. 5. The switch resonator is designed and built using a step-wise waveguide widening with a slit for penetration of the e-beam into the resonator. The slit center is situated opposite the sharp edge of the cathode at the field maximum in the $TE_{0n}$ mode. A high-voltage pulse fed to the cathode injects the e-beam into the switch resonator, resulting in a change in its resonance frequency, and thus in the reflection coefficient of the switch.

The operating principle of the switch can be understood from the frequency characteristics of the iris, reflector and switch, as shown in Fig. 6a, without, and 6b, with, the e-beam in the reflector. In the regime of energy storage the reflector is in resonance and its reflection coefficients is as in curve 1 and in the iris shown in curve 2 determine the reflection coefficient of the switch (curve 3, in Fig. 6a). When the e-beam is injected the frequency characteristics of the reflector and the switch are as in curves 1 and 3, in Fig. 6b. The position of the resonance minimum for the switch with injected e-beam depends on the electron density, the geometric dimensions of the reflector, and the distance between the reflector and the iris. Thus, by regulating the latter one can change the position of the minimum and, hence, the reflection coefficient $R_d$ in the discharge stage. Thus the switch can vary the total

reflection coefficient, from $R_0$ = 0.9 to $R_d$ = 0.2 when the e-beam is injected into the reflector just before the last time bin.

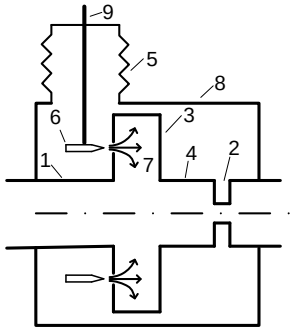


Fig. 5. E-beam switch with reflector and iris: 1 – input circular waveguide, 2 – diaphragm, 3 - stepped widening (reflector), 4 – tunable waveguide, 5 – isolator, 6 – cathode, 7 – e-beam, 8 – vacuum chamber, 9 - electrode.

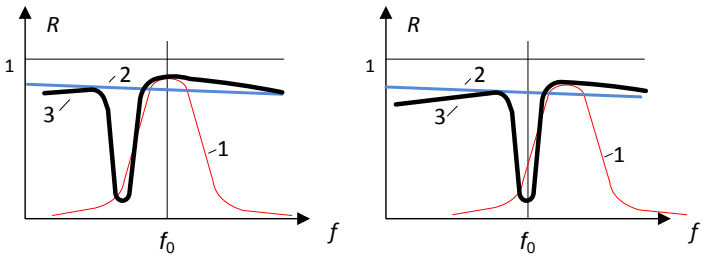


*(a)* *(b)*

Fig.6**.** Total reflection coefficient of $TE_{01}$ mode from the switch (curve 3) without (a); and with (b) electron beam in the reflector.

A second version of the switch is designed similar to that described in ref. [7], where the switches are located at the ends of the delay lines. Microwave energy is stored in high-$Q$ $TE_{02}$ modes, and switched out in the $TE_{01}$ mode. The switches will undergo a sharp increase in the $TE_{02}\rightarrow TE_{01}$ mode conversion coefficient when the e-beams are injected into the switch resonators. The design is modeled by computing interaction of the e-beam with fields of the $TE_{01n}$ mode excited in the switch resonator. Dynamics of the free electron distribution in the switch is calculated by the Particle-in-Cell (PIC) method [8-10] as it was done for the switch shown in Fig. 3b.

Calculations were made of e-beam current versus distance between anode and cathode. The calculated distribution of the injected electrons in the resonator at a beam current 200 A is shown in Fig. 7a. The calculations showed that 80-100% of the electrons emitted by the cathode can be injected into the switch resonator, depending on the anode-to-cathode distance and the width of the cathode edge. The calculation process also allows one to determine the phase and the reflection coefficient $R$ at the switch resonator after e-beam injection, as shown in Fig. 7b. In these calculations, the switch resonator was operating in the $TE_{01}$ mode at $f_0$ = 11.424 GHz. After the oscillations in the switch resonator stabilized (at $t$ ~ 5 ns), an e-beam was injected into the resonator at the time $t^*$ = 25 ns. Dependences of the phase and modulus of the reflection coefficient on the e-beam current varies are shown in Fig.7b. The calculations were performed for $I_1$= 200 A and $I_2$= 400 A.

Fig. 7 shows that injection of the current at the time $t^*$ = 25 ns results in a sharp change in phase of the reflected wave and energy outflow from the switch resonator ($R$ > 1). Here, the increase in current leads to a larger and faster change in phase. The time of phase change $\tau_p$ is determined by the time of stabilization in the switch resonator, namely $\tau_p = Qs/2\pi f_0$. For example, when $Q_S$ = 400, $\tau_p$ ≈ 6 ns. Switch design during Phase I is based on calculations of the sort described here, taking into account the parameters and dimensions of the resonant delay line of SLED II system at SLAC.

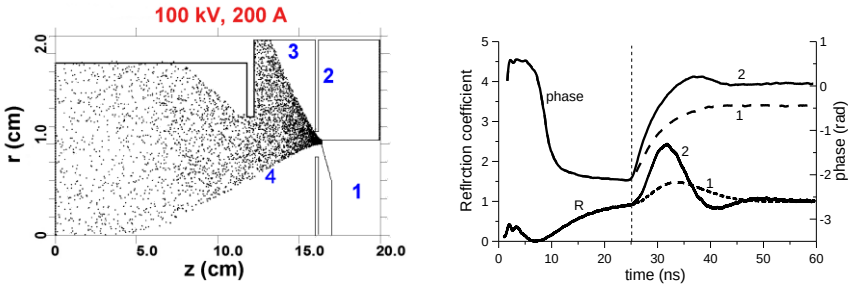


(a) (b)

Fig. 7. (a) Instantaneous calculated distribution of electrons (4) inside the switch resonator (3) at a beam current of 200 A and cathode voltage of 100 kV: 1 – cathode, 2 - anode. (b) Dependence of the phase and modulus of *R* on time, for e-beam currents: 1- $I_1$ = 200 A, and 2 - $I_2$ = 400A.

## III. DEGREE TO WHICH PHASE I HAS DEMONSTRATED TECHNICAL FEASIBILITY

### IIIa. Technical objectives

The technical objectives for Phase I sprang from idea of developing a compact, long-lifetime and super-high-power e-beam switch for a full-scale active SLED II system. This system would have strong potential for applications that include high-power rf breakdown tests of accelerator structures and components and eventual use with high gradient X-band linacs. The overall objective for Phase I was to evolve designs for e-beam switches, fabrication of one type of these switches, and tests of the switch at low power levels. The Work Plan included the following tasks:

***Task 1.*** Development of designs of the two different versions of the e-beam switche based on the two concepts of operation with characteristics required for active SLED II.

***Task 2***. Numerical simulation of operation of various e-beam switches using the FDTD code.

***Task 3.*** Selection, engineering design and fabrication of one of non-vacuum prototypes of the e-beam switches with improved characteristics.

***Task 4.*** Measurements of the switch characteristics at a low power level.

***Task 5***. Experimental investigation of the e-beam switch operation in the scheme similar to active SLED II system.

***Task 6.*** Determination of the maximum output power for the designed e-beam switches.

***Task 7.*** Formulation of the proposal for Phase II, and preparation of the Final Report for Phase I.

Thus the Phase I program was aimed at defining the best design version of the e-beam switch for an active X-band SLED II system, with fabrication and testing of the switch to take place during Phase II, aiming for peak output powers of 300 MW, and efficiency of the system greater than 70%. Collaboration with a SLAC team led by Professor Sami G. Tantawi will be maintained during Phase II. In the following sub-sections of this proposal, results of fulfilling the above tasks are described.

### IIIb. Experimental investigation of the e-beam switch of version 2.

Two versions of e-beam switches have been considered within the project framework. The first version is similar to the flow-through plasma switch tested by us at SLAC [11, 12], but replacing gas-discharge tubes with e-beams. The second version is based on the $TE_{02}$-$TE_{01}$ mode transformation and requires a more significant modification in the design of the SLED-II compressor. This switch was tested successfully by us at NRL at high power levels within the two-channel compressor with a short storage cavity. Consequently, we started our investigation with this version (version 2) of the switch.

Operation of version 2 e-beam switch as a component of a resonant delay line compression system was tested experimentally at a low power level. For this purpose, the length of the storage cavity was 5 m, as compared with the 2 m in experiments at NRL [7]. Thus the round trip group travel time of an electromagnetic wave increased from 22 to 70 ns. The e-beam switch was similar to that

shown in Fig. 6, but modified for operation with a long non-evacuated resonant delay line 70 mm in diameter. A photo of the switch and a diagram of the experimental setup are shown in Fig. 8.

The compression system was formed by coupling device (input and output waveguides, in which the $TE_{02}$ mode is cut off), smooth tapered transitions from diameter of 38 mm to diameter of 70 mm, a cylindrical copper waveguide (delay line) 5m long and 70 mm in diameter, smooth tapered transitions from diameter of 70 mm to diameter of 50 mm and the e-beam switch of version 2. The input horn, cylindrical waveguide, and switch form a storage cavity for the $TE_{02}$ mode. The cylindrical waveguide includes a section of variable length, which can be changed using a special mechanical drive so as to tune the cavity to a desired working frequency. The radiation generated by an oscillator into a $TE_{10}$ square-waveguide mode is transformed by Marie mode converter into a $TE_{01}^{O}$ mode and fed to the input of a compressor at 11.424 GHz. Thus, it was identical to the compressor circuit in [2], but the short 2-m storage cavity was replaced with a 5-m resonant delay line.

Frequency characteristic of the compressor was measured using a scalar network analyzer model 8757C. The loaded Q-factor of the storage resonator, as measured experimentally, was $Q_L = (2.2–3.4)\times10^4$, depending on the parameters of the switch resonator. The measured coupling coefficient (parameter $\beta$) of storage resonator was $\beta \sim 1$ and was optimized for CW excitation [4]. The compressor was switched from the regime of microwave power storage into the regime of power output by firing the HV pulser. A high- voltage triangular pulse with amplitude of 140 kV and pulse duration of 30 ns FWHM was fed to the cathode of switch. The distance between the anode and the stainless steel cathode was varied in the range $D_{a\text{-}c}$=2-7.5 mm. The diameter of the cathode was 20 mm, and the cathode had a sharp edge with a thickness of 0.2 mm. The switch was evacuated with an ion pump to a pressure of $10^{-6}$ Torr. Electrons injection resulted in a change in the resonance frequency of the switch resonator, loss of resonance, and, correspondingly, to a variation in the phase of the signal reflected from the resonator. At the same time, the $TE_{02}\rightarrow TE_{01}$ transformation coefficient increased up to the unit. As a result, microwave energy stored in the resonator in the $TE_{02}$ mode was emitted through the input horn in the $TE_{01}$ mode. Fig. 9a shows a typical oscillogram of compressed pulses obtained in our experiments for compressor with resonant delay line.

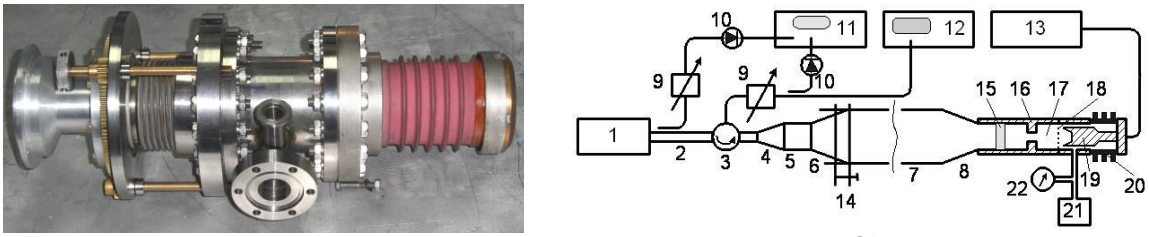


(a) (b)

Fig. 8. a) General view of e-beam switch of version 2; b) Schematic layout of the experiment: *1* – microwave generator, *2* - directional coupler, *3* – circulator, *4* – Marie $TE_{10} \rightarrow TE_{01}^{o}$ mode converter, *5* - cylindrical waveguide, *6* – input-output taper, *7* – storage resonator, *8* – taper, *9* - attenuator, *10* - microwave detector, *11* - oscilloscope, *12* - scalar network analyzer, *13* - HV pulser, *14* - special mechanical drive; *15* - microwave window, *16* - movable diaphragm, *17* – switch resonator, *18* – anode (aluminum foil), *19* – cathode, *20* – insulator, *21* – pumping port, 22 - vacuum gauge.

Fig. 9 shows the compressed pulse with two peaks separated by $\tau$ = 70 ns, the round-trip time around the resonant delay line, and that the output pulses have durations shorter than $\tau$. Analysis shows that such pulse profiles can be observed when the duration $\tau_b$ of the beam current is less than $\tau$. Thus, the first pulse in Fig. 9 corresponds to the compressed pulse produced during injection of the e-beam with duration $\tau_b$. The second pulse is a result of passive compression on the trailing edge of the pulse. Indeed, when the duration of the electron beam is $\tau_b \sim 30$ ns, only the leading part of the microwave pulse with the duration $\tau$ is output from the storage cavity. The trailing edge of this pulse is where passive compression takes place, it is the second pulse in Fig. 9a.

.

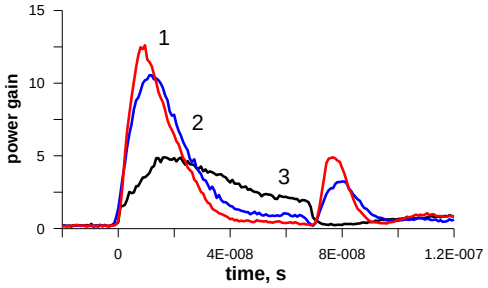


Fig. 9a. Typical oscilloscope traces of the compressed pulses with resonant delay line and switch employing e-beam triggering. The gap between anode and cathode is equal: 1 - 2 mm, 2 – 4 mm, 3 – 7.5 mm

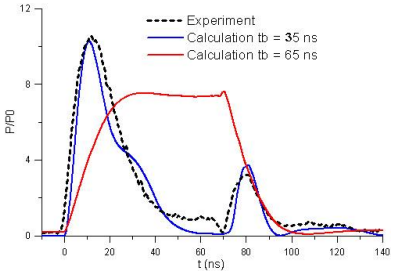


Fig. 9b. Comparison of the experimentally produced compressed pulses with the calculated results: the experiment (dashed line) and calculations for pulse durations of 35 ns and 65 ns, (blue and red line, respectively).

Operation of the compressor with this switch and a delay line 5-m in length and 70-mm in diameter was simulated by the FDTD method; and the spatial distribution of the e-beam in the switch resonator, by the PIC method. Characteristics of the e-beam so calculated were used in the FDTD algorithm to calculate parameters of the compressed pulse. Figure 9b compares the calculated compressed pulse with the experimental one. The two agree for the amplitude of the beam current $I$ = 310 A. In the calculations the current pulse was assumed rectangular, the duration of its plateau was 15 ns, and the pulse decay time was 20 ns, which correlates well with measurements of the profile of the e-beam pulse. Fig. 9b shows the profile of the compressed pulse with a flat plateau duration of 65 ns. It follows that in order to obtain compressed rectangular pulses, one should ensure that the duration of the current pulse exceeds the round-trip time along the delay line. These tests showed that the high-voltage pulse was too short to allow obtaining rectangular profiles of compressed pulses.

It should be noted that the duration of the e-beam injected into the switch resonator is determined by duration of the high-voltage pulse and by the time during which the gap is bridged by the cathode plasma. When cathode plasma is produced, an increase in the gap $D_{a\text{-}c}$ between the cathode and anode can result in longer current durations. One can see from Fig. 9a that with $D_{a\text{-}c}$ = 7.5 mm, the compressed pulse was quasi-rectilinear with duration $\tau$ = 70 ns. As $D_{a\text{-}c}$ increased, a lower power gain was achieved due to a decrease in current caused by a drop in electric-field at the cathode.

Thus, this experiment demonstrated that in order to obtain rectangular pulses in a compressor with a long resonant delay line, one should use high-voltage pulses with durations exceeding the tound-trip time along the delay line, as well as to use an appropriate cathode-anode gap.

### IIIc. Investigation of obtaining e-beam current with required duration

Experiments with the longer delay line and the version 2 e-beam switch demonstrated that current pulses need durations exceeding the round trip time $\tau = 2L/v_g$, where $v_g$ is the group velocity of the $TE_{01}$ mode and $L$ is the length of delay line, to produce rectangular pulses. For the present delay lines of SLED-II, this time is $\tau$ =173 ns. Means for achieving longer beam current durations for the explosive-emission point cathode, which was used in the e-beam switch, was studied using a special setup. A high-voltage pulse generator with amplitude up to 40 kV and duration adjustable from 100 to 1000 ns was used in the tests. The scheme and a photo of the set-up are shown in Fig.10.

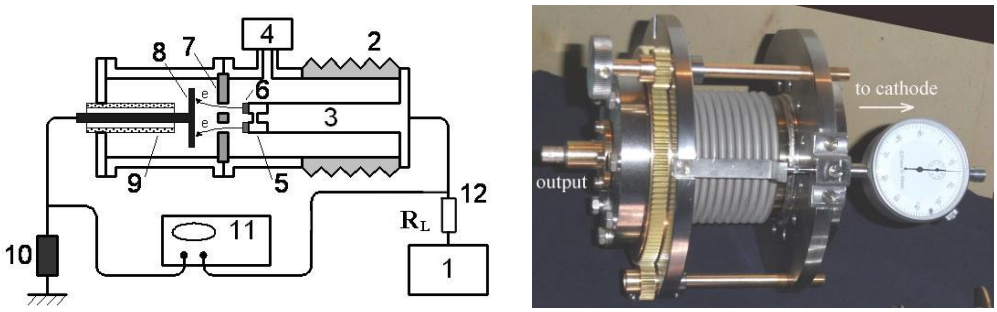


a) b)

Fig.10. (a) Schematic drawing of the experimental setup for field electron emission measurement: 1 – high-voltage pulse generator, 2 – isolator, 3 – cathode holder, 4 – pumping, 5 – movable cathode head, 6 – diamond or related film, 7 – anode (copper disk with slit), 8 – collector, 9 – isolator, 10 – low induction resistor, 11 – scope, 12 - limiting resistor; b) General view of the experimental setup for emission current measurement.

The cathode assembly was tested in a vacuum chamber (at $10^{-6}$ Torr or less), and consists of a cathode holder that supports a disposable cathode head (5). High-voltage pulse generator (1) was connected to the cathode via inductance-free limiting resistor $R_L$. The resistor value was varied in experiment in the range $R_L$ = 0-460 Ohm.The anode is a wire grid (with the cell size 3×3 mm) made out of copper, or a disk with slits cut at some distance from its center. One can move the cathode head along the cathode holder axis, thus regulating the distance between the anode and the cathode (electric field at the cathode). The electrons emitted from the cathode are accelerated in the gap between the anode and the cathode, pass through the slits (grid) in the anode and then are gathered by collector (8). The collector current is measured using non-inductive resistor (10). The distance between the anode and the stainless steel cathode was varied in the range $D_{a\text{-}c}$=1-8 mm. The diameter of the cathode was 20 mm, and the cathode had a sharp edge with a thickness of 0.2 mm. Thus, we could compare the duration of the emission current by changing the distance between the anode and the cathode.

Characteristic oscillograms of the current through the anode slit and the cathode voltage are shown in Fig. 11a for different values of the limit resistance $R_L$. It is seen in the figure that the onset of the emission current is accompanied by a drop in the cathode voltage. This is due to the change in the impedance of the cathode gap when plasma is formed on the cathode tip and the emission current starts. When plasma bridges the cathode gap completely, the cathode voltage drops sharply, almost to zero, and emission stops. Increasing the limit resistance $R_L$ results only in a decrease in the emission current without an increase in its duration. A change in amplitude of the high-voltage pulse from 15 kV to 35 kV does not lead to any significant change in the current pulse duration, a seen in Fig. 11b.

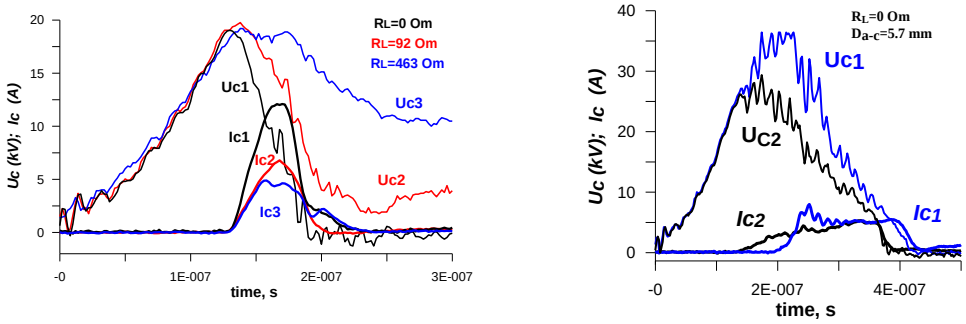


a) b)

Fig. 11. (a) Current and cathode voltage as functions of the limit resistance; and (b) amplitude of the high-voltage pulse .

Thus, the experiments demonstrated that the limitation of the current pulse duration is due to bridging of the cathode-anode gap by the plasma formed on the point of the explosive-emission cathode. It is known [5-6] that the near-cathode plasma expands at the rate $V_p$~(1-2)×$10^6$ cm/s. So the

bridging time would be $\tau_b = D_{a\text{-}c}/V_p$= 50-800 ns depending on the anode-to-cathode distance. Figure 12 shows oscillograms of the emission current for different distances between the anode and cathode and two values of the limit resistance.

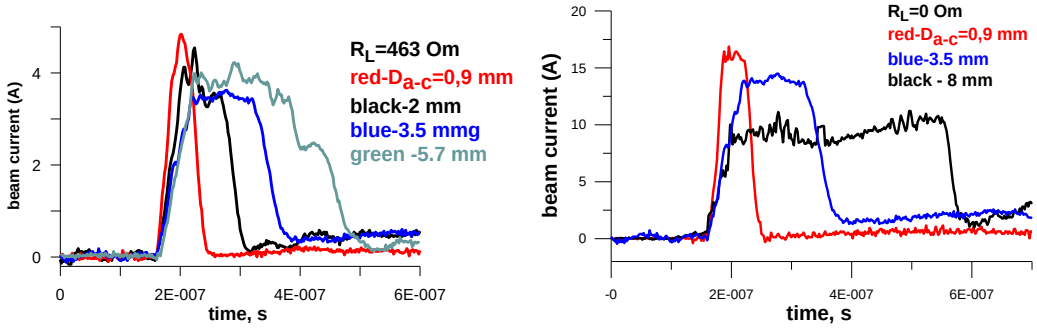


(a) (b)

Fig. 12. Emission current as a function of the distance $D_{a\text{-}c}$ between the anode and the cathode for two values of the limit resistance: $R_L$ = 0 Ω (a) and $R_L$ = 463 Ω (b).

One can see from Fig. 12 that a wider gap between the anode and the cathode results in a longer e-beam pulse passing through the anode diaphragm. This shows the possibility in principle to obtain an e-beam with duration of ~200 ns, which is necessary for the planned experiments with the delay line of the SLED-II system having round-trip time equal to $\tau$ =173 ns. To achieve the required parameters, we are planning during Phase II to build a high-voltage pulse generator with the required duration, and use a switch with an anode-to-cathode distance of more than 5 mm.

### IIId. Design and characteristics of the e-beam switch of version 1

The version 1 e-beam switch consists of a reflector (resonator) and an iris. The main component is the resonator, into which the e-beam is injected. The use of an iris is not mandatory, but it allows reduction of electric fields in the resonator and adjustment of switching coefficient over a wider range as compared to having no iris. Therefore, to check performance of a version 1 e-beam switch, we calculated and built a simplified prototype consisting only of the adjustable cavity, but no iris.

Our version 1 test switch is shown schematically in Fig. 13a. It was designed and built based on a step-wise waveguide widening with a slit (9) for injection of the e-beam. The slit center is situated opposite the sharp edge of the cathode at the field maximum in the $TE_{0n}$ mode excited in the switch resonator. Its frequency characteristic near the operating frequency $f_0$ is shown in Fig. 13b.

At the operating frequency such a reflector has a reflection coefficient $R_0$ close to unity in the regime of energy storage. When the e-beam is injected the frequency characteristics of the reflector shifts and reflection coefficient becomes lower ($R_d$<$R_0$). The position of the resonance curve for the switch with injected e-beam depends on the beam current and the geometric dimensions of the reflector. Thus, by regulating the latter, one can change the position of the minimum and, hence, the reflection coefficient $R_d$ in the discharge stage.

In our experiment the reflector was connected with circular waveguide 38.1 mm in diameter, where only the $TE_{01}$ mode propagated. The reflector of the switch is formed by a step-wise widening of the circular waveguide from a diameter of 38.1 mm to 100 mm. We used the waveguide 1.5" diameter as in SLAC's 11.424 GHz passive SLED-II system, by assuming that e-beam switch could be installed there in place of its iris. Specifications of the e-beam switch with chosen geometric dimensions were calculated numerically by the FDTD method [8-10]. The calculated model is shown in Fig.14. The $TE_{01}$ mode with power $P_0$ propagating only towards the switch is excited in a circular waveguide 38.1 mm in diameter by means of a system of electric and magnetic currents induced in a defined plane. The transmitted wave, $P_1$, and the reflected wave, $P_2$, are absorbed in the absorber, with which the ends of the waveguide are filled. Transmission and reflection coefficients are $|R|^2 = P_2/(P_1+P_2)$ and $|T|^2 = P_1/(P_1+P_2)$, for no wall losses.

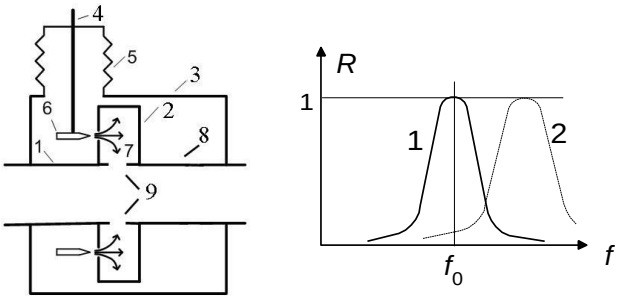


(a) (b)

Fig.13. a) Electron beam switch with reflector on the basis of a step-wise waveguide widening: 1 – input circular waveguide, 2 – stepped widening (reflector), 3 - vacuum chamber, 4 – electrode, 5 – isolator, 6 – cathode, 7 – electron beam, 8 - output circular waveguide, 9 – slit; b) Frequency characteristic of the resonance reflector: 1- in the regime of energy storage; 2- in the regime of energy extraction.

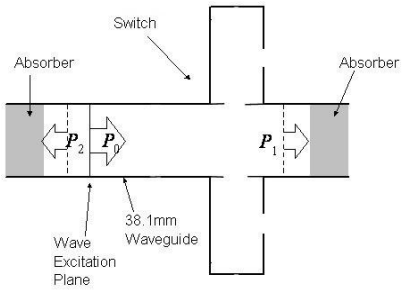


Fig.14. Calculated model of the e-beam switch

Figure 15 shows instantaneous distribution of the electric field in the switch with a single-mode resonator excited at the $TE_{011}$ mode in the regime of energy storage in the resonant delay line and in the regime of energy extraction. In the regime of energy storage a major part of the power is reflected from the switch. When the e-beam is injected, the switch "brightens up" and the reflection coefficient drops sharply. The principle of operation of this switch can be understood from the calculated frequency characteristic shown in Fig.16. In the regime of energy storage the main part of the power is reflected from the switch at the operating frequency $f_0$ = 11.424 GHz. The reflection coefficient from the reflector (step-wise waveguide widening) is high (curve 1). When the e-beam is injected, the frequency characteristic is displaced, and the reflection coefficient decreases (curve 2). Thus, at a frequency of $f_0$ = 11.424 GHz, the switch can provide the required variation of the total reflection coefficient, e.g. from $R_0$ = 0.7-0.9 to $Rd$ = 0-0.3 of the resonant delay line when the e-beam is injected into the reflector just before the last time bin.


a) b)

Fig.15. Instantaneous distributions of the electric field in the switch: a) in the regime of energy storage (high reflection coefficient); b) in the regime of energy output (low reflection coefficient). Here higher intensity corresponds to a higher value of the electric field. 1-storage resonator, 2-switch resonator, 3-output waveguide, 4- injected electron beam.

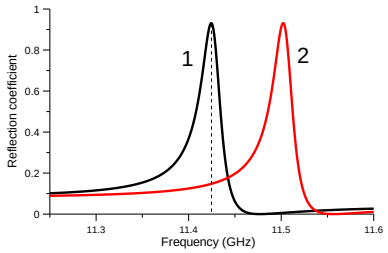


Fig.16. Calculated frequency characteristics of the switch: 1 - in the regime of energy storage (high reflection coefficient); 2 - in the regime of energy output (low reflection coefficient); dash line is working frequency

### IIIe. Experimental study of operation of e-beam switch of version 1

To check performance of the version 1 e-beam switch, we built and tested a prototype. To simplify its design, its resonator did not have a mechanical means for changing its resonance frequency. Therefore, in the process of the low-power experiment, the resonator was tuned by varying the frequency of the microwave generator. The loaded *Q*-factor $Q_L$ of the resonator was determined by the size of coupling slit and $Q_L$ = 385 was chosen. A photograph and drawing of the version 1 e-beam switch are shown in Fig.17.

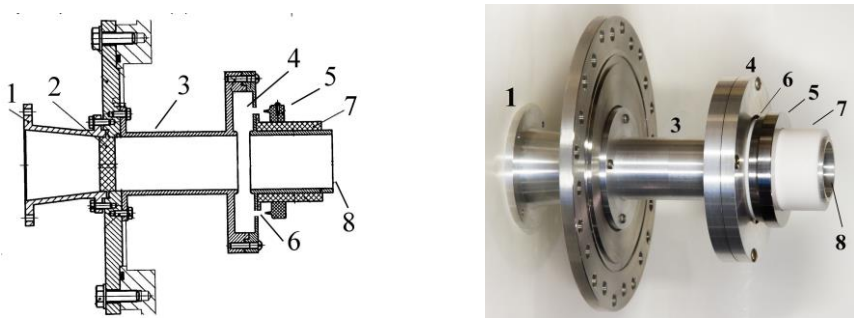


a) b)

Fig.17. (a) The schematic diagram of the e-beam switch of version 1: *1* – input taper, *2* – microwave window, *3* – cylindrical waveguide, *4* – switch resonator, *5* – cylindrical cathode, *6* – anode slit, *7* – isolator, *8* – output waveguide; (b) A photograph of e-beam switch of version 1.

In contrast to the version 2 e-beam switch, we are planning to use a cathode with a much wider diameter (70 mm instead of 20 mm). Therefore, in the experiment we checked whether the electron density in the beam produced by such a cathode was sufficient to bring the switch resonator out of resonance. Operation of the version 1 e-beam switch of was studied using low-power measurements. Results are shown in Fig. 18. The frequency characteristic of the switch without e-beam agrees sufficiently well with the calculated one. The eflection coefficient in the regime of energy storage is $R_0$ = 0.9–0.95 depending on the operating frequency and parameters of the reflector.

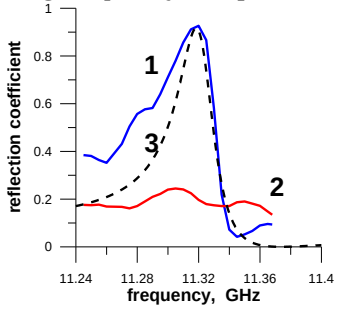


Fig.18**.** Frequency characteristics of the version 1 switch: 1 – measurement (regime of energy storage), 2 – measurement (regime of energy output), 3 –calculation (regime of energy storage).

Switching experiments were performed as follows. The switch resonator was tuned to the working frequency $f_0$ by means of a sweep generator (1). In this case, depending on the chosen frequency, the oscilloscope displayed the signal reflected from the resonator, which corresponded to the reflection coefficient in the vicinity of the resonance curve of the switch, Fig. 18. To produce an e-beam, high-voltage pulses with amplitude 140 kV and duration 40 ns were used. Anode-cathode spacing was $D_{a\text{-}c}$=3 mm. Typical oscillograms of variations of the reflected and transmitted signals upon e- beam injection are shown in Fig.19. As seen, injection leads to a drop in the reflection coefficient from $R_0$ = 0.9–0.95 to $R_d$ = 0.05-0.2. The experiments also show that in the case of non-uniform electron emission from the sharp edge of the cathode, the switch responds well, but the switching coefficient turns out to be lower than in the case of uniform emission (Fig. 19b).

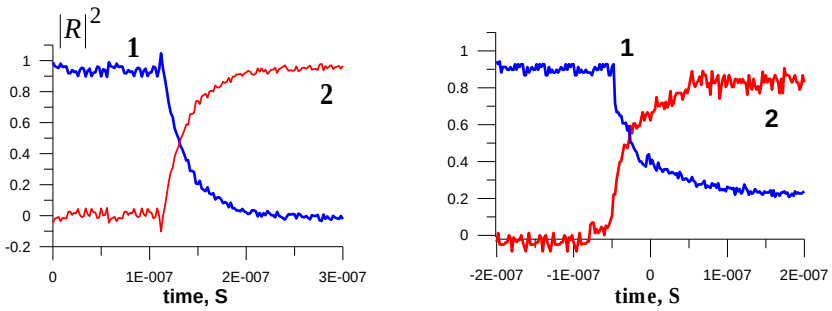


Fig. 19. Characteristic oscillograms of signals reflected (1) and transmitted (2) from the switch when the e-beam is injected. (a) Homogeneous emission from the sharp cathode edge and (b) inhomogeneous emission from the sharp cathode edge.

One sees from Fig. 20 that injection of the e-beam results in the resonator falling out of resonance for a time which significantly exceeds the 40 ns duration of the high-voltage pulse. Evidently, this is due to penetration of the near-cathode plasma into the switch resonator. Note also that uniformity of the electron emission can be improved significantly by using diamond-coated cathodes [11]. Thus, preliminary experiments demonstrated the fundamental possibility of using the version 1 e-beam switch for the active SLED -II compressor to be refined, built, and demonstrated during Phase II.

### IIIf. Expected parameters of active SLED-II compressor

As seen from the previous sections, the design of the version 1 e-beam switch developed by us during Phase I makes it possible to create an active SLED II compressor operating at 11.4 GHz using the same configuration as for our earlier active-passive SLED-II compressor with plasma switches [1], shown in Fig.20.

Output parameters of an active SLED II depend on the length of delay line and the duration of the input pulse from the klystron. We assume in what follows that one X-band SLAC klystron with an output power 25-50 MW will be used for excitation of the delay lines. We also assume that, as it is now, that the klystron pulse width is $T$ = 1.6 μs, and that the output pulse width will be $\tau$ = 173 ns (round trip for the existing delay line).

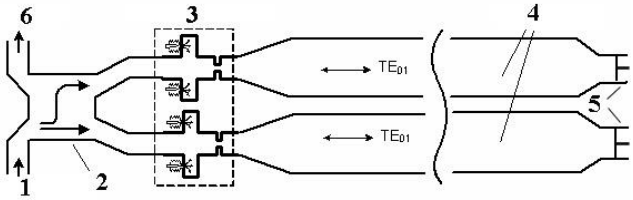


Fig.21. Configuration of an active SLED-II compressor system with version 1 e-beam switches: 1-input waveguide, 2-3dB coupler, 3-e-beam switches, 4-delay line, 5-movable short circuit, 6-output waveguide

Operation of one channel of the active SLED II compressor with the version 1 e-beam switch was simulated numerically. The switch parameters were optimized to fit the parameters of the SLED-II compression system with a long delay line operating in the$TE_{01}$ mode of circular waveguide. The simulation was performed for two variants of pulse compression, namely (1) passive-active compression, where the e-beam injection and phase reversal take place when the time to the end of the input pulse is equal to one round-trip time τ; and (2) active compression without phase reversal, when the beam injection time is at the end of the input pulse. In the case of the passive-active compression, the switching coefficient varies in the range from $R_0 = 0.717$ to $R_d = 0.147$. In the case of the active compression only, its variation is from $R_0 = 0.75$ to $R_d = 0$. Fig. 22 shows the calculated profiles of compressed pulses for the active-passive and purely active SLED II compressor, which were obtained in the case of injection of a 300 A e-beam into the switch resonator. One sees that in both cases that use of the e-beam switch allows one to produce rectangular rf pulses with a power gain $M = 6.5–7$ which exceeds significantly that for passive SLED-II compressor.

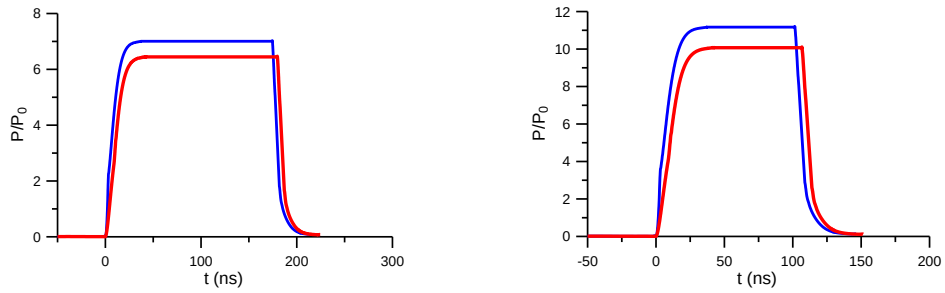


Fig.22. Calculated envelope of the compressed pulse of the SLED-II pulse compression system with the e-beam switch of version 1: (a)- C=9, (b)- C=16; blue – combination of active and passive compression, red – active compression.

So for the e-beam switches, an active SLED II system operating with active-passive compression is predicted to have the following parameters: $R_0 = 0.717$; $\tau = 173$ ns; $C = 9$; and $T = C\times\tau = 1.6$ μs. In this cas Fig.1 predicts a power gain $M = 7$ and efficiency $\eta = 77.5$ %. These parameters are less than they otherwise could be, due to the short input pulse and long delay line. At an input power of 25-50 MW, the peak power would be 175-350 MW. Power gain of would be higher if a delay line of half the length could be used. Parameters would be: $\tau = 86.5$ ns; $C = 18$; $T = C\times\tau = 1.6$ μs; with active-passive compression $M = 12.5$ and $\eta = 69.2$ %; with only active compression $M = 11.6$ and $\eta = 64.5$ %. At an input power of 25-50 MW the peak power would be 300-600 MW.

An active SLED-II system as described here should have strong potential for applications that include high-power rf breakdown tests of accelerator structures and components and eventual use with high gradient X-band linacs.

## V. REFERENCES

1. Wilson P.B., Farkas Z.D., Ruth R.D., SLED II: *A new method of rf pulse compression*, Linear Accel. Conf., Albuquerque, NM, September 1990, SLAC-PUB-5330.
2. Tantawi S.G., Ruth R.D., Vlieks A.E., *Active radio frequency pulse compression using switched resonant delay lines*, Nuclear Instruments and Methods in Physics Research A, 1996, v.370, pp.297-302.
3. O.A. Ivanov, M.A. Lobaev, A.L. Vikharev, A.M. Gorbachev, V.A. Isaev, J.L. Hirshfield, S.H. Gold, and A.K. Kinkead, *Active Microwave Pulse Compressor Using an Electron-Beam Triggered Switch*, Phys. Rev. Letters, v. 110, 115002 (2013).
4. Billy Wiseman Loo, Peter G. Maxim, Valery A. Dolgashev, *Pluridirectional very high electron energy radiation therapy systems and processes*, US Patent Application US 13/765,017, filed 2/12/2013.
5. A.L. Vikharev, O.A. Ivanov, A.M. Gorbachev, M.A. Lobaev, V.A. Isaev, S.G. Tantawi, J.R. Lewandowski, J.L. Hirshfield, Phys. Rev. ST Accel. Beams v. 14, p. 121302 (2011).
6. O.A. Ivanov, V.A. Isaev, M.A. Lobaev, A.L. Vikharev, J.L. Hirshfield, Phys. Rev. ST Accel. Beams, v.14, 061301 (2011).
7. A.L. Vikharev, A.M. Gorbachev, O.A. Ivanov, V.A. Isaev, S.V. Kuzikov, M.A. Lobaev, J.L. Hirshfield, S.H. Gold, and A.K. Kinkead, Phys. Rev. ST Accel. Beams, v.12, 062003 (2009).
8. O.A. Ivanov, V.A. Isaev, M.A. Lobaev, A.L. Vikharev, J.L. Hirshfield, *A resonance switch employing an explosive-emission cathode for high-power RF pulse compressors*, Appl. Phys. Letters, V.97, pp. 031501-031503, (2010)
8. A. Taflove, *Advances in Computational Electrodynamics. The Finite-Difference Time-Domain Method* (Artech, London, 1998).
9. A.B. Pippard, *The physics of vibration*, (Cambridge University Press, New York, 1989).
10. V.P. Tarakanov, *User's Manual for Code KARAT*, Springfield: BRA, 1992.
11. R. A. Alvarez, D. P. Byrne, and R. M. Johnson, Rev. Sci. Instrum. **57**, 2475 (1986)
12. S.D. Korovin, E.A. Litvinov, G.A. Mesyats, A. Murzakaev, V. Rostov, V. Shpak, S. Shunailov, M. Yalandin, Techn. Phys. Lett. 30, 813 (2004).
13. S. Korovin, G. Mesyats, I.V. Pegel, S.D. Polevin, V.P. Tarakanov, IEEE Trans. Plasma Sci. 28, 485 (2000).
14. V.V. Chernov, O.A. Ivanov, V.A. Isaev, D.B. Radishev, A. L.Vikharev, A.V. Kozlov, *High-current electron emission of thin diamond films deposited on molybdenum cathodes*, Diamond & Related Materials, **37**, (2013), 87-91.
15. 2001 Report on the Next Linear Collider, SLAC-R-571, Snowmass 2001. Zeroth-Order Design Report. SLAC Report 474, May 1996.